Published in final edited form as:

Langmuir. 2017 March 21; 33(11): 2770–2779. doi:10.1021/acs.langmuir.6b04116.

Influence of Aqueous Inorganic Anions on the Reactivity of Nanoparticles in TiO_2 Photocatalysis

Jeffrey Farner Budarz[†], **Andrea Turolla**[‡], **Aleksander F. Piasecki**[†], **Jean-Yves Bottero**[§], **Manuela Antonelli**[‡], and **Mark R. Wiesner**[*,†]

[†]Department of Civil and Environmental Engineering, Pratt School of Engineering, Duke University, 27708 Durham, North Carolina, United States

[‡]DICA—Environmental Section, Politecnico di Milano, Piazza Leonardo da Vinci 32, 20133 Milano, Italy

[§]CEREGE, CNRS and Aix-Marseille University, Europole Méditerranéen de l'Arbois, BP80, 13545 Aix en Provence Cedex 04, France

Abstract

The influence of inorganic anions on the photoreactivity and aggregation of titanium dioxide nanoparticles (NPs) was assessed by dosing carbonate, chloride, nitrate, phosphate, and sulfate as potassium salts at multiple concentrations. NP stability was monitored in terms of aggregate morphology and electrophoretic mobility (EPM). Aggregate size and fractal dimension were measured over time by laser diffraction, and the isoelectric point (IEP) as a function of anion and concentration was obtained by measuring EPM versus pH. Phosphate, carbonate, and to a lesser extent, sulfate decreased the IEP of TiO_2 and stabilized NP suspensions owing to specific surface interactions, whereas this was not observed for nitrate and chloride. TiO_2 NPs were exposed to UV-A radiation, and the photoreactivity was assessed by monitoring the production of reactive species over time both at the NP surface (photogenerated holes) and in the bulk solution (hydroxyl radicals) by observing their reactions with the selective probe compounds iodide and terephthalic acid, respectively. The generation of photogenerated holes and hydroxyl radicals was influenced by each inorganic anion to varying degrees. Carbonate and phosphate inhibited the oxidation of iodide, and this interaction was successfully described by a Langmuir–Hinshelwood mechanism and related to the characteristics of TiO_2 aggregates. Chloride and nitrate do not specifically interact with TiO_2, and sulfate creates relatively weak interactions with the TiO_2 surface such that no decrease in photogenerated hole reactivity was observed. A decrease in hydroxyl radical generation was observed for all inorganic anions. Quenching rate constants for the reaction of

[*]**Corresponding Author** wiesner@duke.edu. Phone: (919) 660-5292.

Supporting Information

The Supporting Information is available free of charge on the ACS Publications website at DOI: 10.1021/acs.langmuir.6b04116. Analysis of UV–vis spectra; radiation intensity as a function of emission wavelength at the liquid upper surface; characterization of size distribution of TiO_2 aggregates as a function of operating conditions; aggregation of TiO_2 NPs in inorganic anions; Gouy–Chapman calculations; fractal dimension of TiO_2 NPs; zeta potential versus pH as a function of anion concentration; influence of initial iodide concentration on hole detection; time series for iodide oxidation as a function of inorganic anion concentration; Langmuir–Hinshelwood linearization procedure for K_A and K_R constants estimation; time series for terephthalic acid oxidation as a function of inorganic anion concentration; and normalized hydroxyl radical generation as a function of inorganic anion concentration (PDF)

The authors declare no competing financial interest.

hydroxyl radicals with each inorganic anion do not provide a comprehensive explanation for the magnitude of this decrease, which arises from the interplay of several physicochemical phenomena. This work shows that the reactivity of NPs will be strongly influenced by the makeup of the waters they are released into. The impact of anion species on hydroxyl radical inhibition was as follows: carbonate > chloride > phosphate > nitrate > sulfate.

Graphical Abstract

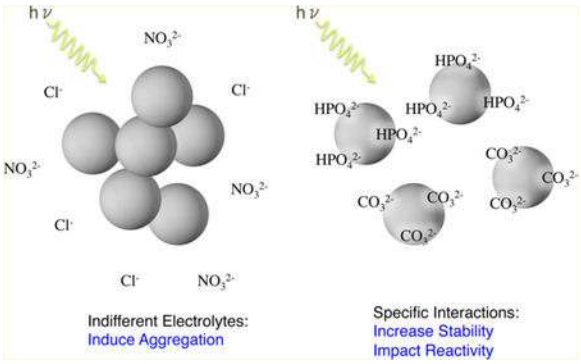

1. INTRODUCTION

Titanium dioxide (TiO_2) nanoparticles (NPs) are widely used in a multitude of commercial products, including food, personal care products, paints, coatings, paper, and fibers owing to their brightness, high refractive index, and UV resistance.[1–4] Applications related to their photoelectrochemical properties are of particular research interest involving solar energy conversion, photocatalytic pollution remediation, and photoinduced superhydrophilicity.[5,6] In particular, TiO_2 NP photocatalysis may be used in water and wastewater treatment, as an advanced oxidation for chemical pollutants or a disinfection process for pathogens based on the generation of reactive species when TiO_2 NPs in suspension are irradiated by photons of wavelength below 390 nm.[7] The potential for TiO_2 photocatalytic degradation of a number of contaminants has already been highlighted,[8,9] though further investigations are required to improve its cost-efficiency and to develop its application at the full scale.[10]

The same photochemical properties that make TiO_2 appealing from an engineering standpoint also have implications for NP release into the environment. TiO_2 NPs are influenced by the presence of many components of natural waters including inorganic anions, which are ubiquitous at significant concentrations.[11,12] Photoexcitation of TiO_2 NPs produces an electron–hole pair that may migrate to the NP surface, where the photogenerated hole can participate in surface oxidation reactions or can abstract an electron from hydroxide, producing the hydroxyl radical. The impact on TiO_2 reactivity by inorganic anions can be direct: interference with the physicochemical processes leading to reactivity or can be indirect: changes in the NP stability and aggregation state, which in turn alter the reactivity.[7] For the direct mechanism, several studies have been published indicating that inorganic anions influence the fundamental physicochemical processes taking place during TiO_2 photocatalysis, including photon absorption, surface adsorption, and photocatalytic degradation.[13–20] Anions compete for the active sites on TiO_2 surfaces, which can prevent

the reaction of pollutants that must be adsorbed before degradation. The specific adsorption of various anions, such as phosphate, leads to a reduction in the amount of hydroxide ions at the TiO_2 surface, which are the precursors of hydroxyl radicals.[21–24] Furthermore, photocatalytic degradation is inhibited when reactive species are directly quenched by anions. This phenomenon follows the specific reactivity of each compound with the generated reactive species.[25] Given the difficulty in differentiating the chemical reactions involved, reactivity assessments have generally been limited to monitoring model contaminant degradation, such as dyes or organic solvents, whose reaction pathways are complex and mostly unknown.

Similarly, most studies assessing the influence of inorganic ions on the reactivity of TiO_2 suspensions have been carried out without a detailed characterization of TiO_2 aggregates that would provide the information on the importance of the indirect mechanism. The influence of inorganic anions on NP aggregation has been extensively documented for NP diffusion and transport in aquatic systems.[26–30] This area of research is of particular interest because of the increasing concern for environmental implications of nanomaterials. In particular, the interactions among TiO_2 NPs can often effectively be described by DLVO theory, which accounts for van der Waals attraction and electrical double layer repulsion in determining the potential for aggregation.[29,31,32] Generally, the repulsive energy of the electric double layer is dominant for TiO_2 NPs in water. This energy barrier decreases with increasing ionic strength, corresponding to double layer compression, which decreases the electrostatic repulsion. As a result, the ionic strength of the solution can be related to the stability of electrostatically stabilized NP suspensions.[27] Though some work has looked at the impact of aggregate size and structure on reactivity, there remains a lack of understanding of how ionic species and concentration influences the characteristics of TiO_2 suspensions and their reactivity.

In this work, the reactivity of TiO_2 suspensions in the presence of inorganic species was assessed on a laboratory scale, by monitoring the reaction of reactive species with probe compounds. Using highly selective chemicals (previously described in several publications[33–35]) allows one to assess the specific influence of inorganic ions on the availability of various reactive species in the development of radical pathways. Specifically, the oxidation of iodide (dosed as potassium iodide, KI) to iodine (I_2) was used to monitor photogenerated holes (h^+), and hydroxylation of terephthalic acid (TA) to 2-hydroxyterephthalic acid (2-HTA) was used to detect hydroxyl radicals ($OH^\bullet$). The products of these reactions are easily measurable by spectrometric and fluorimetric techniques.[36] TiO_2 NP suspensions were prepared via probe sonication, and the inorganic species (carbonate, chloride, nitrate, phosphate, and sulfate) were dosed as potassium salts at several concentrations. TiO_2 suspensions were photoactivated by UV-A irradiation, and the reactive species concentrations were evaluated over time along with TiO_2 aggregate characterization. This research has strong implications not only for TiO_2 photocatalysis engineering but also for the assessment of the risk related to the environmental release of the engineered nanomaterial.

2. MATERIAL AND METHODS

2.1. Reagent Solutions.

KOH, KI, I_2, $KHCO_3$, KCl, KNO_3, KH_2PO_4, K_2HPO_4, and K_2SO_4 were purchased from VWR International (USA). Stock solutions of inorganic anions (0.1 M) were prepared in deionized (DI) water for carbonate. The starch solution was prepared by adding 0.5 g of starch (VWR International) in 100 mL of boiling DI water and mixing until complete dissolution. After 12 h settling, the supernatant was collected. TA (0.5 mM) and 2-HTA (0.125 mM) solutions were prepared by dosing 16.72 mg of TA (Sigma-Aldrich, USA) and 4.69 mg of 2-HTA (Sigma-Aldrich) in 200 mL of DI water, adjusting pH to 7.9 with KOH, and mixing on a magnetic stir plate overnight.

2.2. TiO_2 Dispersion and Suspension Characterization.

Experiments were performed with P25 Aeroxide TiO_2 NPs (Evonik, Germany). TiO_2 stock suspensions (40 mg L^{-1}) were prepared by adding 2 mg of P25 TiO_2 to 50 mL of DI water and stock solutions of inorganic anions, depending on the test conditions. Following the protocol of Taurozzi et al., NPs were dispersed via probe sonication (Q700, QSonica, USA) for 6 min in the pulse mode (12 s ON/3 s OFF) with 1/2″ diameter tip in the presence of a low concentration of inorganic anions (1 mM).[37] pH was adjusted to 7.9 with KOH (0.1 M) after sonication, and the remaining inorganic anions were added to the desired concentration afterward when stocks were diluted in the reaction beaker.

Laser diffraction (Mastersizer 3000, Malvern Instruments, England) was used to determine TiO_2 aggregate size and fractal dimension. Inline light scattering measurements were recorded using a peristaltic pump located downstream of the instrument by which samples were fed from a beaker continuously mixed on a magnetic stirrer at 400 rpm. Time-resolved size measurements, reported in terms of median diameter (D_{50}) both as number-weighted and volume-weighted intensity, were taken every 2 min for 30 min. Meanwhile, static light scattering (SLS) measurements, consisting of measurements of the scattering intensity, $I(q)$, over a range of scattering vectors, q, corresponding to 0.8–42° for each sample were recorded simultaneously by an array of detectors. From eq 1, the aggregate fractal dimension, D_f, can be determined as the negative slope of the linear power law region when plotting $\log(I(q))$ versus $\log(q)$[38]

$$I(q) = q^{-D_f} \quad (1)$$

The multiple detectors of the Mastersizer correspond to scattering vectors from 0.18 to 9.47 μm^{-1}, with q related to the detector angle, λ, as follows

$$q = \frac{4\pi n}{\lambda} \sin\frac{\theta}{2} \quad (2)$$

where n is the refractive index of the medium (1.33 for water) and λ is the wavelength of scattered light (633 nm).[38,39] Equation 2 holds when

$$qR_g > 1 \quad (3)$$

that is, for length scales, (q^{-1}) less than the radius of gyration of the aggregate, R_g. Raw light scattering data exported from the Mastersizer 3000 software were processed using code written for Matlab (Mathworks, USA) to identify the linear power law region and calculate D_f for each aggregation time point according to eqs 1–3. This code can be found and downloaded at www.wiesner.cee.duke.edu/facilities.

TiO_2 NP pH titrations were performed on 50 mL suspensions of 20 mg L^{-1} P25 TiO_2 at various anion concentrations. Suspensions were continually stirred while pH was monitored and adjusted with either 0.01 or 0.1 M KOH or HCl. At each pH step, electrophoretic mobility (EPM) of the NPs was measured (Zetasizer Nano ZS, Malvern Instruments, England). Zeta potential was then calculated by Henry equation. The isoelectric point (IEP) was identified as the pH for which the EPM of a suspension was zero.

2.3. TiO_2 NP Reactivity Measurement.

NP exposure to UV-A was performed in a box equipped with two 15 W fluorescent UV lamps (TL-D 15W BLB SLV, Philips, Netherlands) held at 22 ± 1 °C through the use of a chiller. Samples were placed in 10 mL reaction beakers and continuously mixed on a magnetic stirrer at 400 rpm. The radiation intensity at the liquid upper surface was 1.9 mW cm^{-2}, centered at 365 nm (see Supporting Information 1) and monitored by means of a ILT1400 radiometer equipped with a SEL033 UV-A filter (International Light Technologies, USA). The geometry of the reaction beaker (H = 3.5 cm, Ø = 5 cm) produced a 0.5 cm thickness liquid layer, including the stir bar (3 × 10 mm^2).

2.3.1. Photogenerated Holes.—To evaluate the production of photogenerated holes in the presence of the inorganic anions, reaction beakers containing 20 mg L^{-1} P25 TiO_2, 50 mM KI, and various concentrations of anion (0, 0.5, 1, 2.5, 5, 12.5 mM) were exposed to UV light. Solutions were irradiated for a total of 30 min, and all tests were repeated four times. An aliquot (0.5 mL) was added every 5 min to 0.75 mL of a solution of starch in a 2 mL centrifuge tube. Samples were then centrifuged for 5 min at 12 000 rpm to separate the TiO_2 from the solution. The resultant supernatant (1 mL) was transferred to a plastic cuvette (10 mm optical path), and the absorbance at 585 nm was then measured versus DI water using a spectrophotometer (Cary 100, Agilent, USA). Absorbance values were related to iodine concentration by a standard curve, which was evaluated by spectrometric measures over the range of 0.0125 to 0.125 mM iodine. The concentration of photogenerated holes was stoichiometrically estimated as twice the produced iodine concentration, according to the following reaction

$$2I^- + 2h^+ \rightarrow I_2 \quad (4)$$

2.3.2. Hydroxyl Radicals.—Hydroxyl radical production tests were performed on samples consisting of 20 mg L^{-1} P25 TiO_2, 0.125 mM TA, and various concentrations of inorganic anions (0, 0.5, 2.5, 5, 12.5, 25 mM of carbonate, chloride, nitrate, phosphate, and sulfate) and irradiated for 30 min. All tests were repeated four times. An aliquot (0.5 mL) was added every 5 min to 0.75 mL DI water in a 2 mL centrifuge tube. Samples were then centrifuged for 5 min at 12 000 rpm to separate the TiO_2 from the solution. The resultant supernatant (1 mL) was transferred to a plastic cuvette (10 mm optical path), and the fluorescence was measured (Varian Eclipse fluorometer, Agilent, USA) at an excitation wavelength set to 315 nm and emission maximum at 425 nm. The fluorescence was related to the concentration of 2-HTA by a standard curve by diluting 0.125 mM 2-HTA stock solution to obtain a range from 0.0025 to 0.1 M, adopting the procedure similar to that for the samples. Hydroxyl radical concentrations were estimated by the following reaction, assuming 80% trapping efficiency for •OH by TA[40] and considering sample dilution in DI water

$$\mathrm{TA} + \bullet\mathrm{OH} \rightarrow 2 - \mathrm{HTA} \quad (5)$$

3. RESULTS AND DISCUSSION

The strong influence of inorganic anions on TiO_2 NP photocatalysis, resulting from the combination of chemical–physical phenomena is presented here first in terms of impacts on NP aggregation (section 3.1). The anion influence on TiO_2 reactivity is then discussed in terms of photogenerated holes (section 3.2.1) and hydroxyl radicals (section 3.2.2).

3.1. TiO_2 Aggregate Characterization.

UV–vis spectra were obtained for 20 mg L^{-1} TiO_2 in DI water, as well as 25 mM A^- and 50 mM I^- (see Supporting Information 1). The spectra were analyzed to estimate the band gap energy. It is expected that the nanoparticulate nature of P25 should allow direct transitions, in which the absorption of UV light results in the promotion of an electron directly from the valence band to the conduction band without the aid of a phonon (indirect transition).[41,42] Calculation of the band gap energy was performed according to the method described by Calandra et al.,[42] using the classical relation of absorbance, A, near the band edge of a semiconductor

$$A \propto \frac{\left(h\nu - E_g\right)^n}{h\nu} \quad (6)$$

where $h\nu$ is the energy of a photon, E_g is the band gap energy, and the value of n is either 2 for allowed direct transitions or 1/2 for indirect transitions.

Using the UV–vis spectra for 20 mg L^{-1} P25 in DI water, Figure 1a, and considering direct transitions, a band gap of 3.17 eV is determined by extrapolation of the linear segment of the curve when $(A \times h\nu)^2$ is plotted versus $h\nu$, Figure 1b. The determined band gaps for allowed direct transitions in each suspension are given in Table S1 NEXT and shown in Figure

S1.2a–f. The average band gap calculated across all suspensions was 3.13 ± 0.03 eV. This agrees well with previously reported values for P25 of 3.15–3.25[41–45] and suggests that the fraction of rutile (E_g = 3.0 eV) in P25 may be contributing to the absorbance of longer wavelengths, resulting in a lower calculated band gap than that of anatase (3.2 eV).

Sonicating TiO_2 NPs in DI water created aggregates with a stable number weighted D_{50} of 0.095 ± 0.004 μm and volume weighted D_{50} increasing from 0.591 ± 0.296 to 6.84 ± 7.63 μm over 30 min (data in Figure S3). The difference in values arising from the weighting methods is due to the polydispersity of TiO_2 suspensions, indicating that the vast majority of aggregates exist at the smaller size class with relatively few large aggregates influencing the volume weighted D_{50}. This smaller fraction is expected to be the most photoactive, as nonreactive oxygen species (ROS) producing pathways (e.g. quenching, recombination) increase in frequency with aggregation.[46] Suspensions in DI water were repeated five times; the large standard deviation associated with the volume weighted D_{50} arises from the instability of the TiO_2 aggregates in the mixed solution.

3.1.1. Aggregation in Inorganic Salts.—Monitoring TiO_2 D_{50} in the presence of inorganic salts yielded two contrasting trends (i) anions that did not limit NP destabilization and (ii) anions that stabilized NP suspensions through specific surface interactions. Figure 2 shows TiO_2 aggregation over time for each anion at 0.5 and 25 mM at pH 7.9. Aggregates in chloride and nitrate aggregated significantly over 30 min at all concentrations, increasing from an initial TiO_2 number weighted D_{50} similar to that of aggregates suspended in DI water to a final size of a micron or more (data in Figure S4.2). On the other hand, phosphate, carbonate, and sulfate had a stabilizing effect. The greatest effect was seen for phosphate for which no increase in aggregate size was observed, even at concentrations as high as 25 mM. Some aggregation proceeded for suspensions containing carbonate at 12.5 and 25 mM. The addition of sulfate in solution did result in a decrease in aggregation, though this was much less pronounced than for either phosphate or carbonate, and did not exhibit concentration dependence over the range examined.

Looking at the initial rate of aggregation for chloride (Figure 3) and nitrate (Figure S4.2), no clear influence of ionic strength can be discerned, although the attachment efficiency, α, is generally expected to increase with salt concentration until it reaches unity when the critical coagulation concentration (CCC) is reached. DLVO calculations using the Gouy Chapman approximation indicate that attractive forces dominate (i.e. $\alpha = 1$) for 12.5 and 25 mM potassium chloride (data in Figure S5). However, for the lower three concentrations (0.5, 2.5, and 5 mM), the electrical double layer remains large enough that electrostatic repulsion should hinder aggregation. A more detailed explanation of the DLVO calculations can be found in the Supporting Information 5. These results agree well with Solovitch et al. who determined the CCC for 50 mg L^{-1} anatase at pH 8 in unmixed experiments to be between 10 and 40 mM NaCl.[47] No difference was observed in the initial aggregation rates here, despite the differences in particle stability, which highlights the strong influence of mixing the aggregation rate under these conditions. The initial aggregation reached a plateau after approximately 14 min; presumably this is the point at which breakup and reordering due to shear becomes significant. Similarly, the formation of quasistable particle size distributions was observed by Gardner et al. in studying hematite particle aggregation in a Couette device.

[48] For suspensions to which carbonate was added, the initial rate of aggregation was greater for samples at 25 mM than for samples at 12.5 mM of concentration, as would be expected under DLVO theory, though the aggregate size for both quickly stabilizes after which no further aggregation is observed.

3.1.2. Fractal Dimension.—SLS measurements were collected for each aggregation experiment. At early time points, the size of the aggregates is small compared with the length scales probed, and plots of log(I) versus log(q) were not linear over a large enough range of the scattering vectors considered (0.110–5.62 μm) (data in Supporting Information). Hence, the constraint of eq 3 is not met, and related light scattering data were not sufficient to calculate D_f. Furthermore, as no aggregation was observed for any phosphate concentration and for low carbonate concentrations (<12.5 mM), fractal dimensions were not obtainable. For suspensions in which aggregation was observed, the average D_f values over the final three measurements (26–30 min) are shown in Figure 4. Broadly, D_f values were lower for suspensions that were observed to quickly aggregate (nitrate—2.33 ± 0.01, chloride—2.32 ± 0.02, and sulfate—2.31 ± 0.02 for 25 mM), indicative of more open aggregates. Conversely, the higher fractal values for carbonate (2.40 ± 0.02 for 25 mM) agree well with the slower observed aggregation that would result in smaller, denser aggregates. The concentration of anion in solution did not significantly influence the aggregate structure. For nitrate, chloride, and sulfate, values of D_f are observed to center around 2.3 and fall within the range of what is considered to be reaction-limited aggregation, indicative of stable particles. This likely arises from shear due to mixing, resulting in aggregate breakup and reordering, leading to denser clusters. This lack of concentration dependence also agrees well with initial rates of aggregation discussed previously.

3.1.3. Aggregate IEP.—To identify if the various anions influenced the surface chemistry of TiO_2 aggregates, NP suspensions were titrated versus pH with EPM measured for each anion. From these data, the IEP for each suspension was identified (data in Figure S7). The influence of phosphate and carbonate on EPM at 0.5 mM is illustrated in Figure 5a. As can be seen in Figure 5b, the addition of chloride and nitrate, generally considered indifferent electrolytes, did not significantly impact the IEP at any concentration studied (6.6 ± 0.1 vs 6 ± 1[49]), while carbonate and phosphate interacted strongly with the surface, resulting in large shifts in the IEP, the extent of which varied with anion concentration. Sulfate depressed the IEP from that of chloride and nitrate to 5.6 ± 0.2 but did not vary greatly with concentration. However, the impact of carbonate was drastic. At 0.005 and 0.05 mM, the IEP mirrored that of sulfate, though increasing the concentration decreased the IEP to a low of 2.8 at 5 mM. The IEP then rebounded with a further increase in carbonate concentration. Phosphate proved to even more strongly influence the IEP as the concentration increased from 0.005 to 0.5 mM, at which point NPs were negatively charged for the entire range of pH measured. Increasing the phosphate concentration resulted in a slight increase in the IEP, though this was not as pronounced a recovery as was observed with carbonate. Titrations above 12.5 mM were not performed as the ionic strength interfered with EPM data quality.

That carbonate, phosphate, and sulfate were able to influence the IEP speaks for their ability to participate in the inner sphere ligand exchange with the surface oxides and hydroxides present on TiO_2.[50–52] The magnitude of anion influence increases with surface coverage and depends on the dissociation and binding constants of the species present.[13,53,54] The increase in IEP observed for phosphate and carbonate at concentrations of 5 mM and higher may be due to the changes in ligand complexation. Inner sphere complexes can form mono-, bi-, or tridentate complexes depending on the ligand type, pH, lattice structure, and surface defects.[45,55–57] These complexes are associated with different binding energies and associated protonation pK_a values.[53,58,59] As concentration increases and the more energetically favorable binding sites become filled, adsorption will transition to less favorable sites. Phosphate has been shown to favor the bidentate complex formation, with the surface of TiO_2 becoming protonated at low pH. Monodentate adsorption results in a protonated complex that becomes doubly protonated at low pH.[53] The addition of sulfate quickly reaches a maximum impact beyond which further introduction in solution has little to no effect, suggesting that the interactions of sulfate with the surface are less significant than phosphate and carbonate. These data fit well with the observations of aggregate size (section 3.1.2), in which TiO_2 suspended in phosphate and low concentrations of carbonate does not induce aggregation over the course of 30 min, in contrast to nitrate and chloride. Hence, the anions participating in specific surface interactions with TiO_2 strongly influence the stability of the NPs and the size of the aggregates formed in solution.

Both aggregate size and fractal dimension have been demonstrated to influence the photoreactivity of an NP suspension. In studies using TiO_2 and ZnO NPs, aggregation caused a decrease in •OH generation on a per monomer basis, which was effectively modeled as a function of both the decrease in absorption of incident light and the increase in quenching and electron–hole recombination.[60] In addition to aggregate size, the fractal dimension strongly influenced the reactivity of the material on a per monomer basis. This impact on reactivity is due to the changes in mass transport that depend on the aggregate morphology, as well as decreased absorption of light as particles in the interior of the aggregate are shielded from the incident light by those at the surface.

3.1.4. Influence of Photogenerated Hole Detection Method.—KI was used as the probe compound for photogenerated hole oxidation. The addition of KI resulted in NP aggregation from an initial size similar to NPs in DI water (0.099 ± 0.004 μm, number weighted D_{50}) to 1.23 ± 0.56 μm over 30 min (0.547 ± 0.105 μm increasing to 31.13 ± 8.23 μm, volume weighted D_{50}) (data in Figure S3.2). The initial rate of this aggregation was indistinguishable from that observed for nitrate and chloride, discussed previously (data in Figure S4.2).

Size data, both as number weighted and volume weighted D_{50}, over time for TiO_2 suspensions at various iodide concentrations (0, 50 mM) and relative size distributions are reported in the Supporting Information. While the probe itself induces aggregation, it does not do so in a manner that is appreciably different from the addition of the indifferent electrolytes. No significant aggregation was observed in the presence of terephthalic acid; thus, aggregate size data were identical to that for DI water.

3.2. TiO_2 Photoreactivity.

3.2.1. Photogenerated Holes.—The influence of inorganic anions on the production of photogenerated holes was assessed via the oxidation of iodide. The initial KI concentration was determined by measuring the response at various concentrations using suspensions of TiO_2 in DI water (data in Figure S8).[36,61] A saturation trend in oxidation was observed, and 50 mM was selected for use. The high concentration of iodide required to reach saturation likely arises from the negative surface charge of TiO_2 at pH 7.9, both electrostatically limiting iodide transport to the aggregate surface and resulting in an increased concentration of hydroxide ions present in solution and at the NP surface.

Upon addition of the various anions, a change in the rate of iodide oxidation was only observed in the presence of carbonate and phosphate. Chloride, nitrate, and sulfate at concentrations between 0.5 and 12.5 mM did not cause any significant change in iodide oxidation from samples containing only KI. The experimental results after 30 min of irradiation at various carbonate and phosphate concentrations are shown in Figure 6. Experimental data for chloride, nitrate, and sulfate were not significantly different from the results obtained for TiO_2 suspensions without inorganic ions and are not shown. Oxidized iodide concentrations for these three anions overlap the results obtained when only KI is present in solution (data in Figure SI9). The lack of statistically significant differences between series with or without anions for chloride, nitrate, and sulfate was verified by means of Student's t-test (p-value < 0.005).

The addition of carbonate and phosphate increased the rate of hole oxidation for phosphate at concentrations up to 5 mM and for all carbonate concentrations tested as compared to the solutions containing only the probe. The largest increase was observed at 0.5 mM and was the same as that for carbonate and phosphate anions, after which increasing the concentration reduced hole oxidation to a level observed in DI suspensions. These findings agree with the trend of aggregate stabilization reported in section 3.1.2, which would result in increased reactivity, and suggests that at low concentrations, little negative effect on reactivity due to specific surface interactions would be expected. The reduction in reactivity observed with increasing anion concentration is attributed to the presence of phosphate or carbonate occupying surface sites and preventing iodide from interacting with the photogenerated holes. The effect of phosphate addition was greater than carbonate, despite observed aggregation of carbonate at 12.5 mM, indicating that the decrease in photogenerated holes is primarily due to the greater surface interactions of phosphate and TiO_2.

The interactions between anions and TiO_2 NPs have been described by Chen et al., as a Langmuir type adsorption model.[14] The oxidation of iodide can thus be modeled as a Langmuir–Hinshelwood (LH) mechanism, even when considering the presence of other anions in solution, where oxidation takes place in a two-step process of adsorption followed by reaction, described by eq 7.[61]

$$r = \frac{d[I^-]}{dt} = -K_R \cdot \theta_{I^-} = -K_R \cdot \frac{K_{A,I}[I^-]}{1 + K_{A,I}[I^-] + \sum_{anion} K_{A,anion}[\text{ anion }]} \quad (7)$$

Here, r is the reaction rate, θ_{I-} is the surface coverage by iodide, $[I^-]$ is the concentration of iodide, $K_{A,I}$ is the equilibrium constant of adsorption for iodide, $K_{A,anion}$ is the equilibrium constant of adsorption for a given anion, and K_R is the LH reaction constant for iodide oxidation. Estimates of $K_{A,I}$ and K_R were calculated from the experimental data reported in Figure S3 in the absence of other anionic species following the procedure employed by Herrmann and Pichat (see Supporting Information 10), the results of which are shown in Table 1.[61] The high R^2 values indicate that the LH mechanism is appropriate for describing iodide oxidation. These values are comparable with those obtained previously for iodide oxidation in nonsonicated suspensions of TiO_2 at 40 mg L^{-1}.[36]

Similarly, the LH mechanism was used to model the effect of inorganic anions on the formation of photogenerated holes. Here, it is essential to take into account the competition for the active sites in the LH mechanism among inorganic anions. A procedure for $K_{A,anion}$ and K_R estimation in the presence of anionic competition for surface adsorption is described in the Supporting Information 10, in which the equilibrium constant of adsorption for iodide was taken from the previous calculation in the absence of other inorganic anions. The LH mechanism fits the experimental data well ($R^2 > 0.950$). Larger values of $K_{A,anion}$ indicate greater active site occupation by a given anion compared with others at the same concentration. Hence, iodide, having the smallest $K_{A,anion}$ value, is the least favored at the TiO_2 surface under the present operating conditions. $K_{A,anion}$ for phosphate was much higher than that for carbonate and indicates a greater affinity for the TiO_2 surface, which serves to more strongly block iodine from the surface and reduce the hole reactivity. $K_{A,anion}$ for nitrate, chloride, and sulfate were not calculated, as no adsorption in the presence of iodide was observed. The influence of the associated cation, that is, potassium, on reactivity was considered negligible, in agreement with previous works.[62]

3.2.2. Hydroxyl Radicals.—The generation of hydroxyl radicals was evaluated by monitoring the fluorescence of 2-HTA as a function of inorganic anion concentration. TA is a selective hydroxyl radical probe, whose reaction occurs via a single step hydroxylation process in the absence of surface adsorption.[33] At pH 7.9, the carboxylic acid groups on TA are deprotonated, and the molecule is electrostatically repulsed from the negatively charged TiO_2 surface.

Concentrations of 2-HTA for various anionic species after 30 min of irradiation are shown in Figure 7a, whereas relative time series are reported in Figure 7b. For all anions, increasing the concentration in solution decreased the amount of ROS detected, as would be expected for potential hydroxyl radical quenchers. However, rate constants for the reaction of hydroxyl radicals with each inorganic anion, available from literature and reported in Table

2, do not provide a comprehensive explanation for this, as the expected impact on •OH detection differs from the experimental results. For example, the given reactivity of sulfate with hydroxyl radicals (1×10^{10} M^{-1} s^{-1}) is 4 orders of magnitude greater than carbonate (8.5×10^{6} M^{-1} s^{-1}), although in this study carbonate produced the greatest decrease in •OH detection and sulfate produced the least.

While phosphate and carbonate have the smallest reaction rates, their introduction decreased total hydroxyl radical production to the greatest extent. This is best explained by considering the conditions that lead to hydroxyl radical generation, that is, photogenerated hole production and aggregate size. Photogenerated hole production is increased at lower concentrations of phosphate and carbonate (Figure 6) owing to specific interactions with the TiO_2 surface that result in the stabilization of the aggregates at smaller sizes. For carbonate, the increased photogenerated hole generation carries through to hydroxyl radical generation; however, this effect is quickly counteracted by •OH scavenging when increasing the carbonate concentration. Phosphate produces a strong initial decrease in •OH generation at 0.5 mM despite the observed aggregate stabilization and increase in hole production, after which the impact of additional anion is relatively small. Indeed, by 12.5 mM, the quenching •OH detection for carbonate is equal that of phosphate. By 25 mM, the addition of carbonate decreased •OH production by approximately 70%. This greater effect of carbonate than phosphate, in contrast to what is observed for hole oxidation, is likely due to the order of magnitude increase in $k_{\bullet OH}$ for carbonate. Furthermore, the strong impact of both anions, given their relative inactivity with •OH compared with sulfate, chloride, and nitrate (greater than 2 orders of magnitude smaller reaction rate), is attributable to their being drawn to and interacting with the TiO_2 surface. This not only limits the number of surface hydroxides capable of reacting with the photogenerated hole to produce •OH but also increases the local concentration of quenching agents (carbonate and phosphate) near the NP surface relative to tests using the same concentrations of the other anions, thus decreasing both the lifetime of generated hydroxyl radicals.

The trend for nitrate, chloride, and sulfate is more difficult to discern. A large initial decrease in •OH at 0.5 mM compared with DI water is observed for sulfate and nitrate, whereas chloride initially has little discernable impact. Surprisingly, the addition of up to 25 mM sulfate only decreased •OH detection by approximately 3%. Since the interaction between TiO_2 surface and TA is negligible,[33] and TiO_2 aggregate characteristics are similar, the negative influence of nitrate and chloride on terephthalic acid oxidation can be considered to be the result of the interplay of two primary phenomena: (i) a reduction in hydroxyl radical generation because of the occupation of active sites by anionic species instead of hydroxyl ions and (ii) the direct quenching of hydroxyl radicals by inorganic anions. The absorption of incoming photons by inorganic anions resulting in reduced NP photoactivation is considered negligible.[16] The poor description given by the LH mechanism ($R^2 < 0.7$) supports this assertion that the impact on •OH is due to a combination of the phenomena, where mass transfer and electrostatic interactions possibly play a relevant role.

3.3. Discussion.

Previous studies looking at the impact of anions on TiO_2 photocatalysis have monitored the overall degradation of pollutants using the LH mechanism, without differentiating direct hole oxidation from hydroxyl radicals.[13,19] Others, such Chen et al. investigating the degradation of dichloroethylene, assumed adsorption as a necessary precursor to degradation, but ruled out the likelihood of direct hole oxidation.[14] The intensity of inorganic anion influence on TiO_2 reactivity differs in this study from what has been reported, among which, however, there is no general consensus. Differences between studies seem to be strongly related to experimental conditions, namely solution pH, degradation target chemistry, and TiO_2 characteristics (e.g. aggregate size, dispersed vs fixed catalyst), affecting the balance among the involved chemical–physical processes. Indeed, even the morphology of TiO_2 NPs used has been shown to influence photoreactivity due to differences in the exposed crystalline faces.[67] As a result, generalization between studies is difficult. Often, little attempt has been made to discern surface reactivity from bulk oxidation; however, as is evidenced here, the anion impact on hole generation can be different from the impact on ROS generation. Therefore, the mechanism by which a compound or organism is influenced will play a large role in determining the effect of changes in reactivity.

4. CONCLUSIONS

In this work, TiO_2 reactivity has been explored both at the NP surface (photogenerated hole oxidation) and in the bulk solution (•OH detection). Only carbonate and phosphate inhibited the oxidation of iodide through specific surface interactions. Chloride, nitrate, and sulfate either do not interact with TiO_2 or create relatively weak bonds (with respect to carbonate and phosphate) on the TiO_2 surface that do not hinder iodide. For sulfate, it would appear that while the anion does specifically interact with the surface, these interactions are not sufficient to limit iodide from reaching and reacting with the surface. The lack of aggregate stabilization and the measured IEPs corresponding to bare TiO_2 suggest that for nitrate and chloride, no specific interactions take place. The response of •OH reactivity to the addition of anions is more complicated and arises from the multiple existing pathways by which the NPs can be influenced. The overall influence on bulk •OH concentration was observed to follow the trend carbonate > phosphate > nitrate > chloride = sulfate.

This work highlights the fact that the reactivity of NPs will be strongly influenced by the waters they are released into, owing to the interplay of several physicochemical phenomena. Inorganic anion adsorption on the TiO_2 surface happens via a Langmuirian model and creates a competition for active sites with other compounds in solution, both contaminants and hydroxyl ions. The effect of this adsorption can consist of (i) stabilizing NPs, (ii) hindering the interaction of pollutants, and (iii) suppressing hydroxyl radical generation by substituting hydroxyl ions.

Phosphorus concentrations are typically low in natural freshwaters, though the extensive use of fertilizer both in urban and agricultural landscapes creates nearly ubiquitously elevated concentrations in these locations, whereas the natural levels of chloride, nitrate, and carbonate fall easily within the range of concentrations used here.[68–70] These results suggest

that waters containing chloride and nitrate may have relatively little impact on reactivity but will induce aggregation and likely reduce the NP transport, whereas waters containing even low levels of phosphate and carbonate may decrease "acute" reactivity but stabilize NPs such that their lifetime in the water column will be increased. The ultimate impact of NP photoreactivity in environmental waters (risk) will be the combination of reactivity (hazard) and stability or transport (exposure).

Supplementary Material

Refer to Web version on PubMed Central for supplementary material.

ACKNOWLEDGMENTS

Funding for J.F.B. was gratefully provided by the NIEHS-supported Duke University Superfund Research Center (NIEHS grant P42-ES010356). Funding for A.F.P. was gratefully provided by the National Science Foundation (NSF) and the Environmental Protection Agency (EPA) under NSF Cooperative Agreement EF-0830093 and DBI-1266252, Center for the Environmental Implications of NanoTechnology (CEINT). Any opinions, findings, conclusions, or recommendations expressed in this material are those of the author(s) and do not necessarily reflect the views of the NSF or the EPA. This work has not been subjected to EPA review, and no official endorsement should be inferred.

REFERENCES

(1). Hendren CO; Mesnard X; Dröge J; Wiesner MR Estimating production data for five engineered nanomaterials as a basis for exposure assessment. Environ. Sci. Technol 2011, 45, 2562–2569. [PubMed: 21391627]

(2). Weir A; Westerhoff P; Fabricius L; Hristovski K; von Goetz N Titanium dioxide nanoparticles in food and personal care products. Environ. Sci. Technol 2012, 46, 2242–2250. [PubMed: 22260395]

(3). Windler L; Lorenz C; von Goetz N; Hungerbühler K; Amberg M; Heuberger M; Nowack B Release of titanium dioxide from textiles during washing. Environ. Sci. Technol 2012, 46, 8181–8188. [PubMed: 22746197]

(4). Vance ME; Kuiken T; Vejerano EP; McGinnis SP; Hochella MF Jr.; Rejeski D; Hull MS Nanotechnology in the real world: Redeveloping the nanomaterial consumer products inventory. Beilstein J. Nanotechnol 2015, 6, 1769–1780. [PubMed: 26425429]

(5). Carp O; Huisman CL; Reller A Photoinduced reactivity of titanium dioxide. Prog. Solid State Chem 2004, 32, 33–177.

(6). Fujishima A; Zhang X; Tryk D TiO_2 photocatalysis and related surface phenomena. Surf. Sci. Rep 2008, 63, 515–582.

(7). Chong MN; Jin B; Chow CWK; Saint C Recent developments in photocatalytic water treatment technology: A review. Water Res. 2010, 44, 2997–3027. [PubMed: 20378145]

(8). Malato S; Fernández-Ibáñez P; Maldonado MI; Blanco J; Gernjak W Decontamination and disinfection of water by solar photocatalysis: Recent overview and trends. Catal. Today 2009, 147, 1–59.

(9). Choi H; Al-Abed SR; Dionysiou DD; Stathatos E; Lianos P TiO $_2$-based advanced oxidation nanotechnologies for water purification and reuse In Sustainability Science and Engineering; Elsevier B.V., 2010; Vol. 2, pp 229–254.

(10). Lu GQM; Pichat P Photocatalysis and Water Purification: From Fundamentals to Recent Applications; John Wiley & Sons, 2013.

(11). Hotze EM; Phenrat T; Lowry GV Nanoparticle Aggregation: Challenges to Understanding Transport and Reactivity in the Environment. J. Environ. Qual 2010, 39, 1909–1924. [PubMed: 21284288]

(12). Loosli F; Le Coustumer P; Stoll S TiO_2 nanoparticles aggregation and disaggregation in presence of alginate and Suwannee River humic acids. pH and concentration effects on nanoparticle stability. Water Res. 2013, 47, 6052–6063. [PubMed: 23969399]

(13). Abdullah M; Low GKC; Matthews RW Effects of common inorganic anions on rates of photocatalytic oxidation of organic carbon over illuminated titanium dioxide. J. Phys. Chem 1990, 94, 6820–6825.

(14). Chen HY; Zahraa O; Bouchy M Inhibition of the adsorption and photocatalytic degradation of an organic contaminant in an aqueous suspension of TiO_2 by inorganic ions. J. Photochem. Photobiol., A 1997, 108, 37–44.

(15). Burns RA; Crittenden JC; Hand DW; Selzer VH; Sutter LL; Salman SR Effect of inorganic ions in heterogeneous photocatalysis of TCE. J. Environ. Eng 1999, 125, 77–85.

(16). Mehrvar M; Anderson WA; Moo-Young M Photocatalytic degradation of aqueous organic solvents in the presence of hydroxyl radical scavengers. Int. J. Photoenergy 2001, 3, 187–191.

(17). Wang K; Zhang J; Lou L; Yang S; Chen Y UV or visible light induced photodegradation of AO7 on TiO_2 particles: The influence of inorganic anions. J. Photochem. Photobiol., A 2004, 165, 201–207.

(18). Habibi MH; Hassanzadeh A; Mahdavi S The effect of operational parameters on the photocatalytic degradation of three textile azo dyes in aqueous TiO_2 suspensions. J. Photochem. Photobiol., A 2005, 172, 89–96.

(19). Guillard C; Puzenat E; Lachheb H; Houas A; Herrmann JM Why inorganic salts decrease the TiO_2 photocatalytic efficiency. Int. J. Photoenergy 2005, 7, 1–9.

(20). Lair A; Ferronato C; Chovelon J-M; Herrmann J-M Naphthalene degradation in water by heterogeneous photocatalysis: An investigation of the influence of inorganic anions. J. Photochem. Photobiol., A 2008, 193, 193–203.

(21). Kerzhentsev M; Guillard C; Herrmann J-M; Pichat P Photocatalytic pollutant removal in water at room temperature: Case study of the total degradation of the insecticide fenitrothion (phosphorothioic acid O,O-dimethyl-O-(3-methyl-4-nitro-phenyl)-ester). Catal. Today 1996, 27, 215–220.

(22). Brown GE; Henrich VE; Casey WH; Clark DL; Eggleston C; Felmy A; Goodman DW; Grätzel M; Maciel G; McCarthy MI; Nealson KH; Sverjensky DA; Toney MF; Zachara JM Metal oxide surfaces and their interactions with aqueous solutions and microbial organisms. Chem. Rev 1999, 99, 77–174. [PubMed: 11848981]

(23). Anderson MA; Malotky DT The adsorption of protolyzable anions on hydrous oxides at the isoelectric pH. J. Colloid Interface Sci 1979, 72, 413–427.

(24). Johnson SB; Brown GE; Healy TW; Scales PJ Adsorption of organic matter at mineral/water interfaces. 6. Effect of inner-sphere versus outer-sphere adsorption on colloidal stability. Langmuir 2005, 21, 6356–6365. [PubMed: 15982042]

(25). Diebold U The surface science of titanium dioxide. Surf. Sci. Rep 2003, 48, 53–229.

(26). Fernández-Nieves A; de las Nieves FJ The role of ζ potential in the colloidal stability of different TiO_2/electrolyte solution interfaces. Colloids Surf., A 1999, 148, 231–243.

(27). French RA; Jacobson AR; Kim B; Isley SL; Penn RL; Baveye PC Influence of ionic strength, pH, and cation valence on aggregation kinetics of titanium dioxide nanoparticles. Environ. Sci. Technol 2009, 43, 1354–1359. [PubMed: 19350903]

(28). Keller AA; Wang H; Zhou D; Lenihan HS; Cherr G; Cardinale BJ; Miller R; Ji Z Stability and aggregation of metal oxide nanoparticles in natural aqueous matrices. Environ. Sci. Technol 2010, 44, 1962–1967. [PubMed: 20151631]

(29). Petosa AR; Jaisi DP; Quevedo IR; Elimelech M; Tufenkji N Aggregation and deposition of engineered nanomaterials in aquatic environments: Role of physicochemical interactions. Environ. Sci. Technol 2010, 44, 6532–6549. [PubMed: 20687602]

(30). Shih Y-H; Liu W-S; Su Y-F Aggregation of stabilized TiO_2 nanoparticle suspensions in the presence of inorganic ions. Environ. Toxicol. Chem 2012, 31, 1693–1698. [PubMed: 22639241]

(31). Derjaguin B; Landau L The theory of stability of highly charged lyophobic sols and coalescence of highly charged particles in electrolyte solutions. Acta Physicochim. URSS 1941, 14, 633–652.

(32). Verwey EJW; Overbeek JTG Long distance forces acting between colloidal particles. Trans. Faraday Soc 1946, 42, B117–B123.

(33). Ishibashi K-I; Fujishima A; Watanabe T; Hashimoto K Detection of active oxidative species in TiO_2 photocatalysis using the fluorescence technique. Electrochem. Commun 2000, 2, 207–210.

(34). Bartosz G Use of spectroscopic probes for detection of reactive oxygen species. Clin. Chim. Acta 2006, 368, 53–76. [PubMed: 16483560]

(35). Soh N Recent advances in fluorescent probes for the detection of reactive oxygen species. Anal. Bioanal. Chem 2006, 386, 532–543. [PubMed: 16609844]

(36). Turolla A; Piazzoli A; Budarz JF; Wiesner MR; Antonelli M Experimental measurement and modelling of reactive species generation in TiO_2 nanoparticle photocatalysis. Chem. Eng. J 2015, 271, 260–268. [PubMed: 27885321]

(37). Taurozzi JS; Hackley VA; Wiesner MR Preparation of a Nanoscale TiO_2 Aqueous Dispersion for Toxicological or Environmental Testing; NIST Special Publication, 2012; Vol. 1200, p 3.

(38). Bushell GC; Yan YD; Woodfield D; Raper J; Amal R On techniques for the measurement of the mass fractal dimension of aggregates. Adv. Colloid Interface Sci 2002, 95, 1–50. [PubMed: 11843188]

(39). Raper JA; Amal R Measurement of Aggregate Fractal Dimensions Using Static Light Scattering. Part. Part. Syst. Charact 1993, 10, 239–245.

(40). Ishibashi K.-i.; Fujishima A; Watanabe T; Hashimoto K Quantum yields of active oxidative species formed on TiO_2 photocatalyst. J. Photochem. Photobiol., A 2000, 134, 139–142.

(41). López R; Gómez R Band-gap energy estimation from diffuse reflectance measurements on sol–gel and commercial TiO_2: A comparative study. J. Sol-Gel Sci. Technol 2012, 61, 1–7.

(42). Calandra P; Lombardo D; Pistone A; Liveri VT; Trusso S Structural and optical properties of novel surfactant-coated Yb@ TiO_2 nanoparticles. J. Nanopart. Res 2011, 13, 5833–5839.

(43). Hurum DC; Agrios AG; Gray KA; Rajh T; Thurnauer MC Explaining the enhanced photocatalytic activity of Degussa P25 mixed-phase TiO_2 using EPR. J. Phys. Chem. B 2003, 107, 4545–4549.

(44). Tan L-L; Ong W-J; Chai S-P; Mohamed AR Band gap engineered, oxygen-rich TiO_2 for visible light induced photocatalytic reduction of CO_2. Chem. Commun 2014, 50, 6923–6926.

(45). Luschtinetz R; Frenzel J; Milek T; Seifert G Adsorption of phosphonic acid at the TiO_2 anatase (101) and rutile (110) surfaces. J. Phys. Chem. C 2009, 113, 5730–5740.

(46). Hotze EM; Bottero J-Y; Wiesner MR Theoretical Framework for Nanoparticle Reactivity as a Function of Aggregation State. Langmuir 2010, 26, 11170–11175. [PubMed: 20527955]

(47). Solovitch N; Labille J; Rose J; Chaurand P; Borschneck D; Wiesner MR; Bottero J-Y Concurrent aggregation and deposition of TiO_2 nanoparticles in a sandy porous media. Environ. Sci. Technol 2010, 44, 4897–4902. [PubMed: 20524647]

(48). Gardner KH; Theis TL; Young TC The significance of shear stress in the agglomeration kinetics of fractal aggregates. Water Res. 1998, 32, 2660–2668.

(49). Kosmulski M The significance of the difference in the point of zero charge between rutile and anatase. Adv. Colloid Interface Sci. 2002, 99, 255–264. [PubMed: 12509117]

(50). Velikovská P; Mikulášek P The influence of Cl^-, SO_4^{2-} and PO_4^{3-} ions on the ζ-potential and microfiltration of titanium dioxide dispersions. Sep. Purif. Technol 2007, 58, 295–298.

(51). Nelson BP; Candal R; Corn RM; Anderson MA Control of surface and ζ potentials on nanoporous TiO_2 films by potential-determining and specifically adsorbed ions. Langmuir 2000, 16, 6094–6101.

(52). Kazarinov VE; Andreev VN; Mayorov AP Investigation of the adsorption properties of the TiO_2 electrode by the radioactive tracer method. J. Electroanal. Chem. Interfacial Electrochem 1981, 130, 277–285.

(53). Connor PA; McQuillan AJ Phosphate adsorption onto TiO_2 from aqueous solutions: An in situ internal reflection infrared spectroscopic study. Langmuir 1999, 15, 2916–2921.

(54). Kormann C; Bahnemann DW; Hoffmann MR Photolysis of Chloroform and Other Organic Molecules in Aqueous Titanium Dioxide Suspensions. Environ. Sci. Technol 1991, 25, 494–500.

(55). Stumm W The inner-sphere surface complex: A key to understanding surface reactivity. In Advances in Chemistry Series; American Chemical Society, 1995; Vol. 244, Chapter 1, pp 1–32.

(56). Liao L-F; Lien C-F; Shieh D-L; Chen M-T; Lin J-L FTIR study of adsorption and photoassisted oxygen isotopic exchange of carbon monoxide, carbon dioxide, carbonate, and formate on TiO_2. J. Phys. Chem. B 2002, 106, 11240–11245.

(57). Kwon KD; Kubicki JD Molecular orbital theory study on surface complex structures of phosphates to iron hydroxides: Calculation of vibrational frequencies and adsorption energies. Langmuir 2004, 20, 9249–9254. [PubMed: 15461514]

(58). Linsebigler AL; Lu G; Yates JT Photocatalysis on TiO_2 Surfaces: Principles, Mechanisms, and Selected Results. Chem. Rev 1995, 95, 735–758.

(59). Hug SJ; Bahnemann D Infrared spectra of oxalate, malonate and succinate adsorbed on the aqueous surface of rutile, anatase and lepidocrocite measured with in situ ATR-FTIR. J. Electron Spectrosc. Relat. Phenom 2006, 150, 208–219.

(60). Jassby D; Budarz JF; Wiesner M Impact of Aggregate Size and Structure on the Photocatalytic Properties of TiO_2 and ZnO Nanoparticles. Environ. Sci. Technol 2012, 46, 6934–6941. [PubMed: 22225505]

(61). Herrmann J-M; Pichat P Heterogeneous photocatalysis. Oxidation of halide ions by oxygen in ultraviolet irradiated aqueous suspension of titanium dioxide. J. Chem. Soc., Faraday Trans. 1 1980, 76, 1138.

(62). Rincon A Effect of pH, inorganic ions, organic matter and H_2O_2 on E. coli K12 photocatalytic inactivation by TiO_2: Implications in solar water disinfection. Appl. Catal., B 2004, 51, 283–302.

(63). Buxton GV; Greenstock CL; Helman WP; Ross AB Critical Review of Rate Constants for Reactions of Hydrated Electrons, Hydrogen Atoms and Hydroxyl Radicals ($\bullet OH/\bullet O^-$) in Aqueous Solution. J. Phys. Chem. Ref. Data 1988, 17, 513–886.

(64). Katsumura Y; Jiang PY; Nagaishi R; Oishi T; Ishigure K; Yoshida Y Pulse radiolysis study of aqueous nitric acid solutions: Formation mechanism, yield, and reactivity of NO_3 radical. J. Phys. Chem 1991, 95, 4435–4439.

(65). Kochany J; Lipczynska-Kochany E Application of the EPR spin-trapping technique for the investigation of the reactions of carbonate, bicarbonate, and phosphate anions with hydroxyl radicals generated by the photolysis of H_2O_2. Chemosphere 1992, 25, 1769–1782.

(66). Holcman J; Løgager T; Sehested K Reactions of peroxodisulphate and SO_4^- with selected radicals in aqueous solution. Laboratory Studies on Atmospheric Chemistry, 1992.

(67). Dufour F; Pigeot-Remy S; Durupthy O; Cassaignon S; Ruaux V; Torelli S; Mariey L; Maugé F; Chanéac C Morphological control of TiO_2 anatase nanoparticles: What is the good surface property to obtain efficient photocatalysts? Appl. Catal., B 2015, 174, 350–360.

(68). Paul MJ; Meyer JL Streams in the urban landscape. Annu. Rev. Ecol. Syst 2001, 32, 333–365.

(69). Crittenden JC; Trussell RR; Hand DW; Howe KJ; Tchobanoglous G MWH's Water Treatment: Principles and Design; John Wiley & Sons, 2012.

(70). Nikanorov A; Brazhnikova L Water chemical composition of rivers, lakes and wetlands. In Types and Properties of Water; Eolss Publishers Co. Ltd., 2009; Vol. 2, pp 42–80.

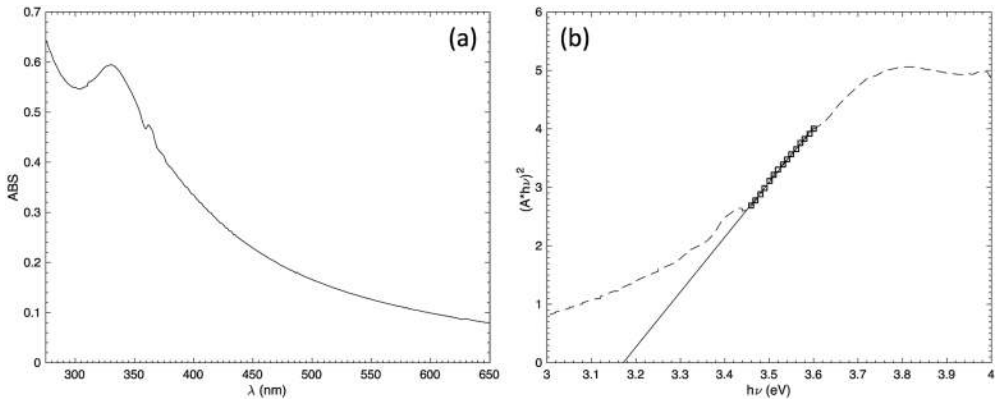

Figure 1.
(a) UV–vis spectra and (b) plot of $(A \times h\nu)^2$ vs $h\nu$ for TiO_2 in DI water.

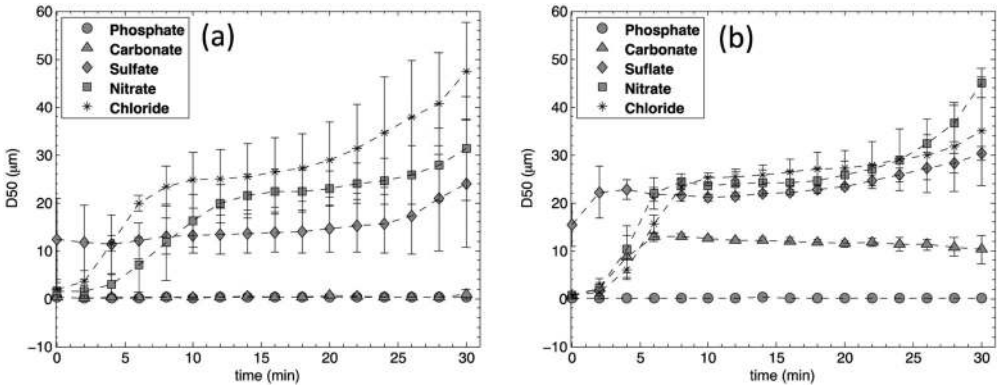

Figure 2.

TiO_2 aggregation over time for each anion at 0.5 mM (a) and 25 mM (b). Data shown are volume weighted D_{50} (mean ± SD).

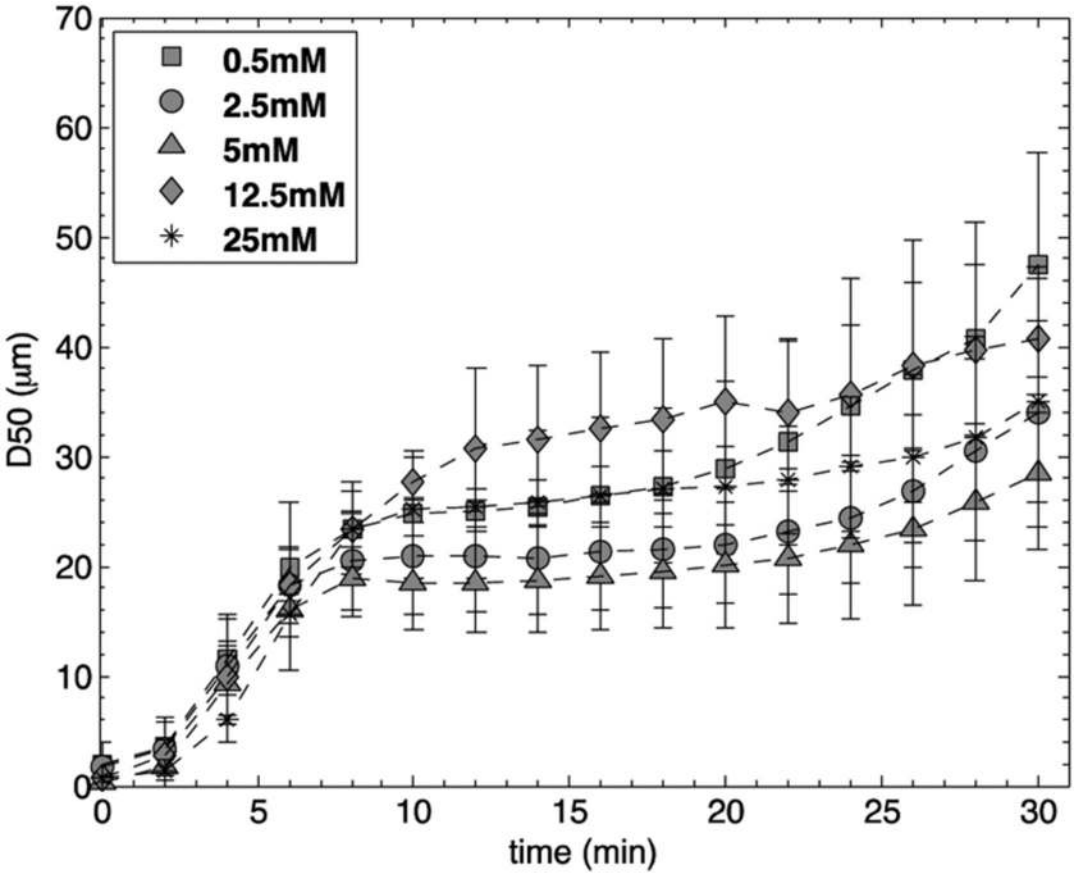

Figure 3.

TiO_2 aggregation (volume weighted D_{50} mean ± SD) vs time as a function of chloride concentration.

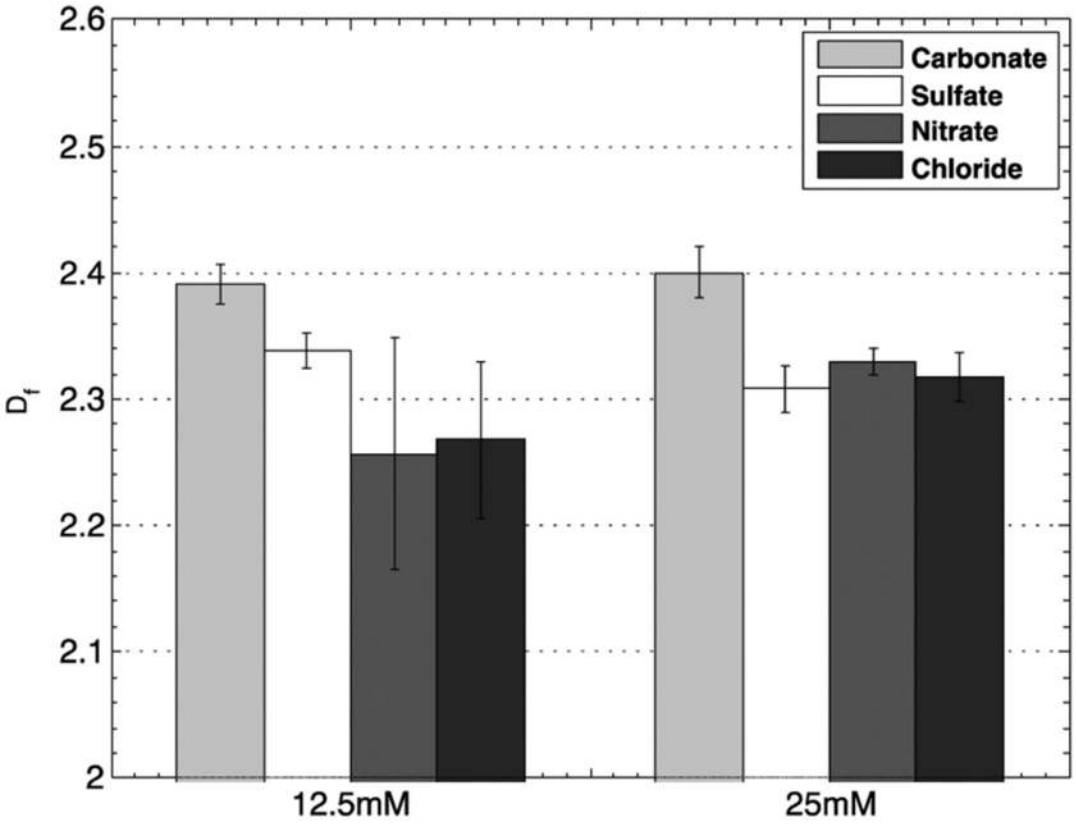

Figure 4.

Fractal dimension of TiO_2 aggregates for all anions at 12.5 and 25 mM. D_f values are the average of final 3 measurements (mean ± SD).

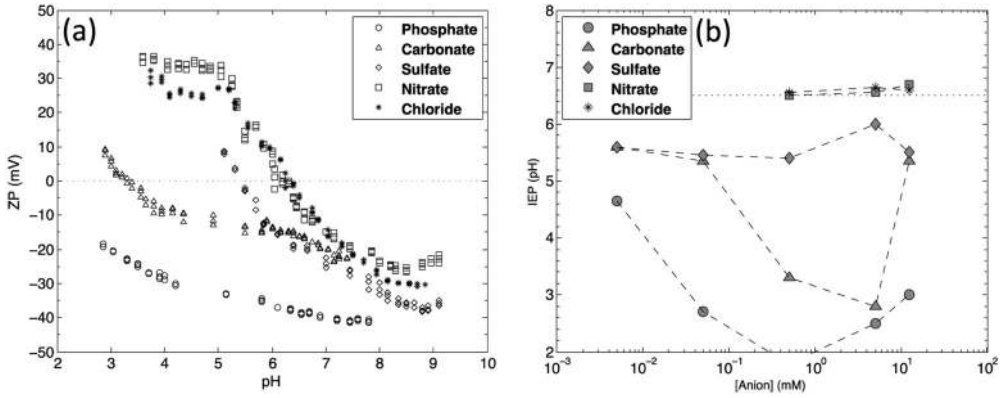

Figure 5.

(a) Zeta potential vs pH for all anions at 0.5 mM. (b) IEP vs concentration for all anions. IEP for 0.5 mM phosphate was not determined as the zeta potential was negative over the range of pH tested.

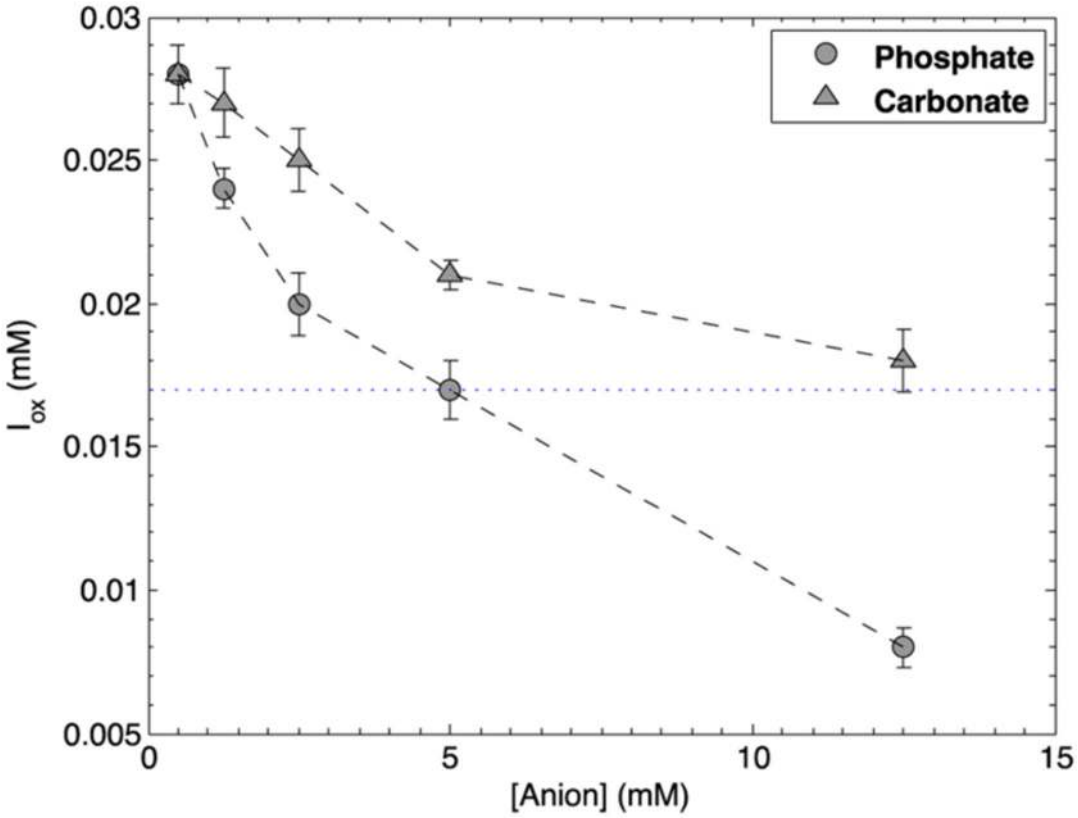

Figure 6.

Oxidized iodide concentration (mean ± SD) vs inorganic anion concentration after 30 min irradiation (50 mM KI) as a function of species in solution (carbonate and phosphate). The blue dotted line is the iodide concentration of TiO_2 suspension containing only 50 mM KI.

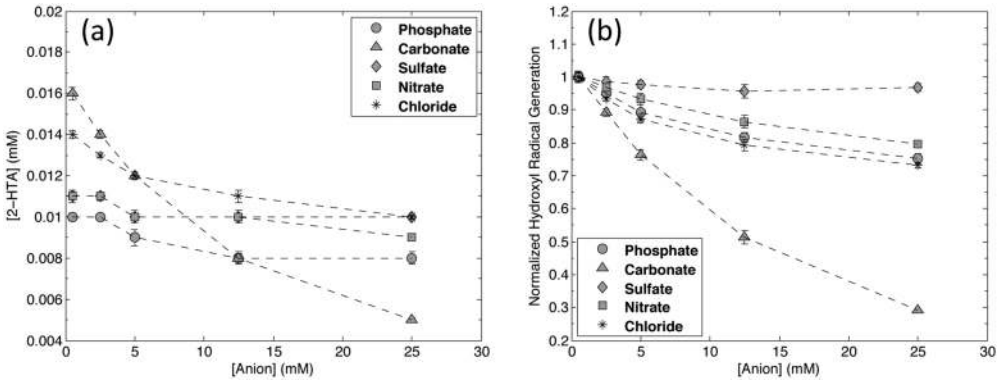

Figure 7.

(a) 2-Hydroxyterephthalic acid concentration (mean ± SD) vs inorganic anion concentration after 30 min irradiation as a function of species in solution. (b) Hydroxyl radical generation normalized to 0.5 mM anion concentration (mean ± SD).

Table 1.

Estimated Values of the Equilibrium Adsorption Coefficient, K_A, for Iodide, Carbonate, and Phosphate and Estimated Values of LH Reaction Constants for Iodide Oxidation, K_R[a]

ionic species	K_A (M^{-1})	K_R ($M\ s^{-1}$)	R^2
iodide	13.2	2.24×10^{-8}	0.988
carbonate	142.7	4.16×10^{-8}	1.000
phosphate	251.8	4.02×10^{-8}	0.954

[a] R^2 values are the coefficients of determination.

Table 2.

Rate Constants from Literature of Hydroxyl Radicals and Selected Inorganic Anions

anionic species	value (M^{-1} s^{-1})	reference
HCO_3^-	8.5×10^6	63
CI^-	4.3×10^9	63
NO_3^-	1.4×10^8	64
HPO_4^{2-}	6×10^5	65
SO_4^{2-}	1.0×10^{10}	66